J. Fluid Mech. (2023), *vol*. 962, A25, doi:10.1017/jfm.2023.281

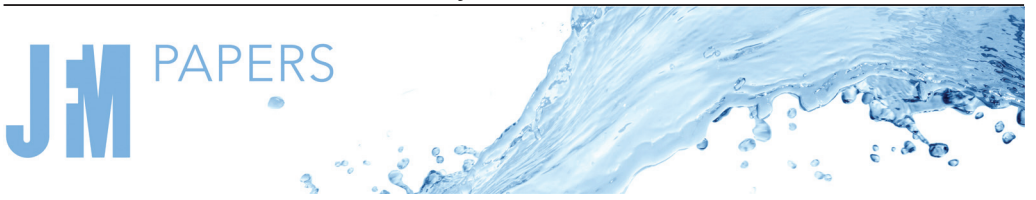

Fundamental time scales of bubble fragmentation in homogeneous isotropic turbulence

Declan B. Gaylo[1], **Kelli Hendrickson**[1] **and Dick K.P. Yue**[1,†]

[1]Department of Mechanical Engineering, Massachusetts Institute of Technology, Cambridge, MA 02139, USA

(Received 20 October 2022; revised 28 March 2023; accepted 30 March 2023)

We investigate the fundamental time scales that characterise the statistics of fragmentation under homogeneous isotropic turbulence for air–water bubbly flows at moderate to large bubble Weber numbers, We. We elucidate three time scales: τ_r, the characteristic age of bubbles when their subsequent statistics become stationary; τ_ℓ, the expected lifetime of a bubble before further fragmentation; and τ_c, the expected time for the air within a bubble to reach the Hinze scale, radius a_H, through the fragmentation cascade. The time scale τ_ℓ is important to the population balance equation (PBE), τ_r is critical to evaluating the applicability of the PBE no-hysteresis assumption, and τ_c provides the characteristic time for fragmentation cascades to equilibrate. By identifying a non-dimensionalised average speed $\bar{s}$ at which air moves through the cascade, we derive $\tau_c = C_\tau \varepsilon^{-1/3} a^{2/3}(1 - (a_{max}/a_H)^{-2/3})$, where $C_\tau = 1/\bar{s}$ and a_{max} is the largest bubble radius in the cascade. While $\bar{s}$ is a function of PBE fragmentation statistics, which depend on the measurement interval T, $\bar{s}$ itself is independent of T for $\tau_r \ll T \ll \tau_c$. We verify the T-independence of $\bar{s}$ and its direct relationship to τ_c using Monte Carlo simulations. We perform direct numerical simulations (DNS) at moderate to large bubble Weber numbers, We, to measure fragmentation statistics over a range of T. We establish that non-stationary effects decay exponentially with T, independent of We, and provide $\tau_r = C_r \varepsilon^{-1/3} a^{2/3}$ with $C_r \approx 0.11$. This gives $\tau_r \ll \tau_\ell$, validating the PBE no-hysteresis assumption. From DNS, we measure $\bar{s}$ and find that for large Weber numbers ($We > 30$), $C_\tau \approx 9$. In addition to providing τ_c, this obtains a new constraint on fragmentation models for PBE.

Key words: breakup/coalescence

† Email address for correspondence: yue@mit.edu

1. Introduction

Fragmentation of bubbles by turbulence resulting in transfer of volume from large to small scales through a fragmentation cascade is relevant to a variety of natural and engineering applications. We consider air–water turbulent bubbly flows where the density ratio between that of the bubble (ρ_a) and the surrounding fluid (ρ_w) is $\rho_w/\rho_a \sim 1000$. While these flows often exhibit multiple physical processes that affect the number of bubbles of a given size (e.g. entrainment, degassing, dissolution, coalescence), fragmentation is critical to understanding the size-distribution of bubbles. For typical bubbly flows with macroscopic time scales large compared with those of the underlying turbulence, the distribution of large bubbles often matches an equilibrium fragmentation cascade (Garrett, Li & Farmer 2000; Deane & Stokes 2002; Deike 2022), suggesting that fragmentation dominates and rapidly reaches equilibrium. Applicable to flows with large Reynolds numbers where the length scale of the bubbles is much larger than the Kolmogorov scale but much smaller than the geometric length scales of the flow, fragmentation of bubbles within the Kolmogorov inertial subrange of homogeneous isotropic turbulence (HIT) is often studied. Recent work has shown that HIT is observed at the bubble scale even in close proximity to a free surface (Yu *et al.* 2019).

In HIT, fragmentation is primarily governed by the disturbing effect of turbulent fluctuations and the restoring effect of surface tension. The ratio between the two is given by the bubble Weber number

$$We = \frac{2\varepsilon^{2/3}(2a)^{5/3}}{(\sigma/\rho_w)}, \tag{1.1}$$

where ε is the turbulent dissipation rate, a is the parent-bubble radius and σ is the surface-tension coefficient. As bubbles are not generally spherical, radius, a, of a bubble here is defined in terms of the volume, v, of the bubble by $a = (3v/4\pi)^{1/3}$. The Hinze scale is defined as the Weber number We_H (and corresponding radius a_H) below which surface tension largely prevents fragmentation (Hinze 1955). Thus, our focus is moderate ($We \gtrsim We_H$) to large ($We \gg We_H$) Weber numbers where fragmentation is present.

For $We \sim \infty$, the daughter bubbles of a previous fragmentation will themselves fragment, leading to an equilibrium fragmentation cascade with bubble-size distribution $N(a) \propto a^{-10/3}$ (Garrett *et al.* 2000). Here, $N(a)\delta a$ is defined to be the number of bubbles of radius $a \leq a' < a + \delta a$. Using location as an analogy for bubble size, for finite We the flux of air due to fragmentation can be either local, corresponding to daughter bubbles of similar size as the parent bubble and likely to further fragment, or non-local, corresponding to daughters much smaller than the parent and likely smaller than a_H (Chan, Johnson & Moin 2021*b*). Chan *et al.* (2021*c*) measure bubbles $We \sim 20$ and demonstrate the locality of the majority of the flux, confirming the applicability of the fragmentation cascade and associated $-10/3$ power law for moderate and large We, where surface tension is present but does not prevent fragmentation. This $-10/3$ power law is observed in a variety of flows including emulsions (Skartlien, Sollum & Schumann 2013), breaking waves (Deane & Stokes 2002) and turbulent free-surface entrainment (Yu, Hendrickson & Yue 2020). This prevalence illustrates that fragmentation cascades are ubiquitous to turbulent bubbly flows for $We > We_H$, and that, despite these flows being transient, an equilibrium fragmentation cascade is often obtained.

For $We > We_H$ where a cascade is formed, our interest here is the evolution of the bubble statistics, in particular the bubble-size distribution $N(a)$, due to fragmentation. In principle, this evolution can be derived from a (more) complete mechanistic description of fragmentation, which is a subject of active investigation (e.g. Liao & Lucas 2009;

Rivière *et al.* 2021, 2022; Qi *et al.* 2022). In addition to the challenge of disparate mechanistic descriptions, another challenge is that these often describe the behaviour of a bubble as dependent on its history (for example, the two-step process presented by Rivière *et al.* (2022)). Contrarily, statistical modelling of bubble-size distributions, particularly through population balance equations (PBE) often used to model large-scale bubbly flows (e.g. Castro & Carrica 2013), assumes that the statistical behaviour of a bubble is independent of its history, i.e. no hysteresis. The present work complements mechanistic studies by focusing on the fundamental statistics of turbulent fragmentation, quantified through their characteristic time scales. While individual physical mechanisms can also be characterised by time scales, such as the time scale for a sufficiently strong eddy to fragment a bubble (Qi *et al.* 2022) or the time scale for capillary-driven production of sub-Hinze bubbles (Rivière *et al.* 2021, 2022), our focus is on the time scales that characterise the fundamental statistics of fragmentation. Understanding these time scales will directly support the statistical modelling of bubble-size distributions through PBE. Additionally, the understanding provided by these statistical time scales will provide robust ways to compare disparate mechanistic models of fragmentation.

In this work, we elucidate and quantify three fundamental time scales of fragmentation for moderate- to large-*We* HIT. In order of magnitude from small to large, these are: the bubble relaxation time τ_r which characterises the time from when a bubble is formed to when its subsequent dynamics (e.g. the rate of fragmentation) become statistically stationary, the (well-established) bubble lifetime τ_ℓ which characterises the time from when a bubble is formed to when it undergoes fragmentation (Martínez-Bazán, Montañés & Lasheras 1999*a*; Garrett *et al.* 2000), and the convergence time τ_c which characterises the time needed for the air to go from the scale of the largest bubble, radius a_{max}, to the Hinze scale, a_H. In § 2 we examine how these time scales relate to statistical modelling of bubble-size distributions through PBE. In previous work, τ_c could not be described for realistic fragmentation statistics (Deike, Melville & Popinet 2016; Qi, Mohammad Masuk & Ni 2020). In § 3 we develop a Lagrangian mathematical description which provides the speed at which volume moves through the fragmentation cascade. This volume-propagation speed allows us to derive τ_c for realistic fragmentation statistics at large *We*. We prove that, unlike typical fragmentation statistics, the volume-propagation speed can be obtained independent of the time interval used for measurement. In § 4 we perform direct numerical simulations (DNS) of moderate- to large-*We* bubble fragmentation in HIT to quantify the three fundamental time scales we address. In § 5 we discuss new insights provided by the quantification of these time scales: τ_r shows hysteresis can be neglected in PBE; and τ_c provides a new constraint on large-*We* fragmentation models.

2. Three fundamental time scales of fragmentation

To define characteristic time scales of fragmentation, we start by examining the statistics typically used to describe fragmentation. To model the population of bubbles within a flow, the evolution $(\partial N/\partial t)(a, t)$ is often expressed as a Boltzmann-style PBE with source terms S describing the effect of each evolution mechanism: fragmentation, coalescence, entrainment, etc. (Sporleder *et al.* 2012). For fragmentation, this source term is

$$S_f(a, t) = -\Omega(a)N(a, t) + \int_a^\infty \bar{m}(a')\beta(a; a')\Omega(a')N(a', t)\,\mathrm{d}a', \tag{2.1}$$

which includes three fragmentation statistics: $\Omega(a)$ is the fragmentation rate (units time^{-1}); $\bar{m}(a')$ is the average number of daughter bubbles created by fragmentation of a parent of radius a'; and $\beta(a; a')$ is the daughter-size distribution, expressed as a probability distribution function of daughter radius a for a given parent radius a'. As volume is conserved in an incompressible flow, it is useful to represent the daughter-size distribution in terms of a volume ratio $v^* = (a/a')^3$, giving a daughter-size distribution f_V^* related to β by

$$a'\beta(a; a') = 3(v^*)^{2/3} f_V^*(v^*; a'). \tag{2.2}$$

Applying volume conservation, the distribution must satisfy (Martínez-Bazán *et al.* 2010)

$$\bar{m}(a') \int_0^1 v^* f_V^*(v^*; a')\, \mathrm{d}v^* = 1. \tag{2.3}$$

While there is great variety in models for $\bar{m}(a')$ and $\beta(a, a')$ (Liao & Lucas 2009), models for $\Omega(a)$ generally follow

$$\Omega(a) = C_\Omega(We)\varepsilon^{1/3} a^{-2/3}, \tag{2.4}$$

where $C_\Omega(We)$ approaches a constant value $C_{\Omega,\infty}$ as $We \to \infty$. Dimensional analysis shows C_Ω may also depend on Reynolds number and an additional parameter, such as the ratio between parent-bubble radius and the Kolmogorov scale, a/η, implied by Qi *et al.* (2022); however, the power-law scaling in (2.4) is robust at large *We* (Martínez-Bazán *et al.* 2010). Assuming $We \sim \infty$ to neglect surface tension, this scaling can be arrived at mechanistically by dividing the characteristic velocity of the turbulent fluctuations on the scale of a bubble ($\varepsilon^{1/3} a^{1/3}$) by the characteristic length a bubble must deform to fragment (a) (Garrett *et al.* 2000). A model for moderate to large *We* based on the assumption that the rate of fragmentation is proportional to the difference between the deforming force of turbulent fluctuations and the restoring force of surface tension is

$$C_\Omega(We) = C_{\Omega,\infty}\sqrt{1 - We_H/We}, \tag{2.5}$$

with $C_{\Omega,\infty} \approx 0.42$ (Martínez-Bazán *et al.* 1999*a*, 2010). To relate $\Omega(a)$ to measured quantities, let $p_{\mathrm{frag}}(a; T)$ be the probability of fragmentation over some measurement interval T, i.e. the probability a bubble of radius a present at time t will fragment before the next measurement at time $t + T$. If we assume, as is done in PBE, that the fragmentation rate of a bubble is independent of the time since its formation, then

$$p_{\mathrm{frag}}(a; T) = 1 - \exp\left[-T\Omega(a)\right], \tag{2.6}$$

and the expected lifetime $\tau_\ell = 1/\Omega(a)$.

Returning to (2.1), we examine this assumption that the statistics describing fragmentation are independent of bubble age, which we will refer to as the no-hysteresis assumption. This no-hysteresis assumption means that the (statistical) behaviour of a bubble after it is created by fragmentation should be indistinguishable from a bubble that has existed for a much longer time. Physically, this seems unlikely over short time scales, as the young bubble must be significantly deformed from equilibrium. Regardless of the mechanistic explanation for fragmentation (either the result of accumulation of surface oscillations (Risso & Fabre 1998) or a single-sufficiently strong eddy (Martínez-Bazán *et al.* 1999*a*)), we expect a young bubble to be more likely to fragment, violating no-hysteresis.

For PBE modelling, it is desirable to assume the effect of hysteresis is negligible, as this allows fragmentation to be treated as statistically independent events; however, as

expected, the validity of this no-hysteresis assumption depends on the time scale one uses to define fragmentation events (Solsvik, Maaß & Jakobsen 2016). As infinitely small temporal resolution is unobtainable, a finite measurement interval T is inherent in the measurement of fragmentation events from both experiments and simulations (Vejražka, Zedníková & Stanovský 2018; Chan *et al.* 2021*a*). To avoid making the no-hysteresis assumption, we will allow for measured fragmentation statistics to depend on T. We rearrange (2.6) to define the T-dependent fragmentation rate

$$\Omega(a;T) \equiv -\ln\left[1-p_{\text{frag}}(a;T)\right]/T. \tag{2.7}$$

For large *We* where daughter bubbles will eventually fragment, it is clear that $\bar{m}$ must also depend on T, and therefore, by (2.3), so must f_V^*. Thus, let $\bar{m}(a';T)$ be the expected number of daughters present at $t+T$ if the bubble fragments and $f_V^*(v^*;a',T)$ be the size distribution of these daughters. The dependence of these statistics on T makes them difficult to relate to the statistics in (2.1) (Solsvik *et al.* 2016). Although the physical mechanism for the decay of hysteresis is unclear, we posit that there exists a time scale τ_r characterising how long the decay takes, such that $\Omega(a;T\gg\tau_r)=\Omega(a)$ is independent of T. It follows that $\tau_\ell \gg \tau_r$ is required for the no-hysteresis assumption to be valid in PBE.

When modelling the bubble-size distribution, the equilibrium solution ($\partial N/\partial t=0$) may be available, such as for PBE with only a fragmentation source term (Garrett *et al.* 2000) or fragmentation with power-law entrainment, where the size distribution of the bubbles injected by entrainment follows a power law (Gaylo, Hendrickson & Yue 2021). The time, τ_c, it takes to reach these equilibrium solutions is of interest: if τ_c is much less than the time scale over which the flow is transient, we expect an equilibrium fragmentation cascade (generally $N(a)\propto a^{-10/3}$) to be obtained. Gaylo *et al.* (2021) provide an expression for τ_c which allows for arbitrary f_V^* and $\bar{m}$, but its derivation is specific to power-law entrainment. For general fragmentation cascades, τ_c is characterised by the time it takes for the volume of the largest bubble to reach the Hinze scale (Deike *et al.* 2016; Qi *et al.* 2020). This characterisation is useful because it allows τ_c to be measured independent of the evolution of $N(a)$. Additionally, being directly related to fragmentation, it could provide a constraint on the fragmentation statistics in PBE (Qi *et al.* 2020). However, current derivations of τ_c from fragmentation statistics assume that bubbles break into identically sized daughters, ignoring the effect of f_V^*. Although Monte Carlo simulation can be used to determine what τ_c is predicted by given fragmentation statistics (Qi *et al.* 2020), the lack of a general analytic expression relating τ_c to realistic fragmentation statistics precludes the reverse – it is unclear how a given value of τ_c constrains fragmentation statistics.

3. Describing τ_c using a Lagrangian description of fragmentation cascades

In this section, we derive a general analytic expression that relates τ_c to realistic fragmentation statistics. Previous derivations of τ_c assume identical fragmentation and that the life of a bubble is exactly (rather than on the average) equal to τ_ℓ so that the cascade can be treated as a series of discrete deterministic fragmentation events (Deike *et al.* 2016). While this approach provides the general physical scaling of τ_c, it is unable directly relate τ_c to realistic fragmentation statistics. In this section we use a Lagrangian air particle-based mathematical description of the speed at which volume moves through fragmentation cascades to derive τ_c. We note that this is a 'speed' in the abstract sense as it measures how quickly air moves from large bubbles to small bubbles through the fragmentation cascade rather than through physical space. However, this description is useful as, through this speed, τ_c can be related to realistic fragmentation statistics

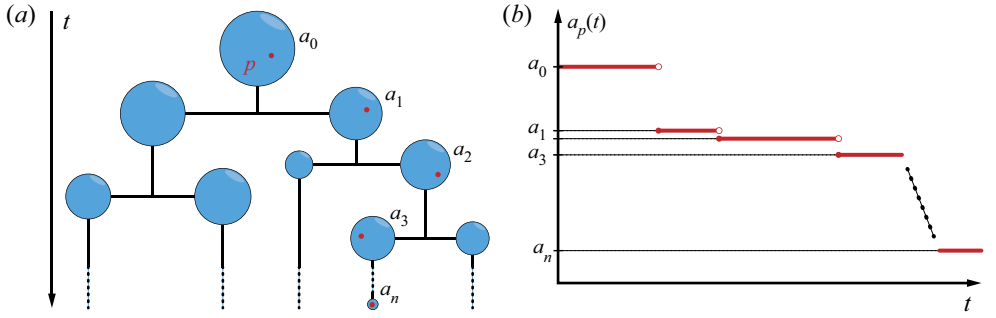

Figure 1. (*a*) Schematic of the Lagrangian description showing the path of a Lagrangian air particle p through a sequence of fragmentations from large to small radii, $a_0, a_1, \ldots, a_n$, of the bubble containing p; and (*b*) the function $a_p(t)$ describing the evolution of this bubble radius. Describing the radius of the bubble containing p as a function of time allows a propagation speed of p through the cascade to be defined.

and this speed is also directly accessible from volume-based bubble-tracking (Gaylo, Hendrickson & Yue 2022). Although T-independence is obvious when τ_c is obtained through the evolution of $N(a)$, it is less clear when τ_c is obtained through fragmentation statistics, which generally depend on T. We show that our approach allows fragmentation statistics-based measurement of τ_c independent of T.

Throughout this section, we consider large We ($We \gg We_H$) so that we can assume that fragmentation statistics are scale-invariant and simplify (2.5) to a Heaviside step function,

$$C_\Omega(We) = C_{\Omega,\infty}\mathcal{H}\left(1 - We_H/We\right). \tag{3.1}$$

In the following derivation, we also assume no-hysteresis, limiting applicability to time scales much larger than τ_r.

3.1. *A Lagrangian-based mathematical description of fragmentation*

Previous work on the movement of volume in fragmentation cascades applies Eulerian descriptions, focusing on volume flux. To find the equilibrium between entrainment and fragmentation, Gaylo *et al.* (2021) balance the flux of volume in and out of the set of bubbles of a given range of sizes. To evaluate locality, Chan *et al.* (2021*b*) study the flux of volume from bubbles larger than a given size to those smaller. Eulerian descriptions are useful to model the volume flow in and out of specified bubble sizes, but to derive τ_c we need to understand how any specific air volume flows through the entire cascade. For this, a Lagrangian description is more direct.

Consider how a single Lagrangian particle of air p moves through a fragmentation cascade, illustrated in figure 1. Let $a_p(t)$ be the effective radius of the bubble that contains p at time t. Treating the interface between fluids as zero-thickness, one bubble breaks up into two instantaneously, thus $a_p(t)$ is a step function. From this $a_p(t)$, we have a simple expression for τ_c: defining time for a particle such that $a_p(0) = a_{max}$, our interest is the expected time for p to reach the Hinze scale,

$$\tau_c \equiv \mathbb{E}\{\min\{t \ : \ a_p(t) \leq a_H\}\}. \tag{3.2}$$

We now develop a relationship between this Lagrangian description and the previous fragmentation statistics. Incorporating the measurement interval T, we define the volume ratio between the bubble containing p at time t and the bubble containing p at time

$t + T$ as

$$v_R(t; T) \equiv [a_p(t + T)/a_p(t)]^3. \tag{3.3}$$

If the bubble containing p at time t does not fragment over the measurement interval T, then $v_R = 1$. If the bubble does fragment, then v_R depends on the size of the daughter bubble that p ends up in. Noting that the probability p ends up in a given daughter is equivalent to v^*, the ratio of the volume of the daughter to that of the parent, the probability distribution function for v_R given that fragmentation occurs, $f_{V_R|\text{frag}}$, is related to the previous fragmentation statistics through

$$f_{V_R|\text{frag}}(v_R; t, T) = \bar{m}(a_p(t); T)\ v_R\, f_V^*(v_R; a_p(t), T). \tag{3.4}$$

We assume these statistics are scale invariant and introduce the non-dimensional parameter $T^* = T\varepsilon^{1/3}a_p(t)^{-2/3}$. This gives

$$f_{V_R|\text{frag}}(v_R; T^*) = \bar{m}(T^*)\ v_R\, f_V^*(v_R; T^*), \tag{3.5}$$

and any moment n of the distribution is given by

$$\mathbb{E}\{[v_R(T^*)]^n \mid \text{frag}\} = \bar{m}(T^*) \int_0^1 v^{*n+1} f_V^*(v^*; T^*)\, \mathrm{d}v^*. \tag{3.6}$$

3.2. *Defining the volume-propagation speed in a fragmentation cascade*

To obtain τ_c, we derive a metric that measures the speed at which Lagrangian air particles move through fragmentation cascades. To derive a speed, we must first define the 'location', $x(t)$, of a Lagrangian air particle p within the cascade. In this case location refers to some scalar bubble-size metric within the cascade rather than a physical spatial coordinate. We define $x(t)$ to describe the location of p within the fragmentation cascade such that the associated speed $s(t) \equiv \dot{x}(t)$ is constant for $a_p(t) > a_H$. A constant speed is necessary for many of the properties that will follow and, as a result of the scaling in (2.4), is achieved only by $x(t) \propto a_p(t)^{2/3}$. We choose

$$x(t) \equiv -\varepsilon^{-1/3}a_p(t)^{2/3}, \tag{3.7}$$

which has dimensions of time, so that, in addition to being constant, the time derivative of $x(t)$,

$$s(t) = -\frac{2}{3}\varepsilon^{-1/3}a_p(t)^{-1/3}\frac{\mathrm{d}}{\mathrm{d}t}a_p(t), \tag{3.8}$$

is also positive and non-dimensional.

Because $a_p(t)$ is a step function, the derivative in (3.8) is ill-behaved. Thus, to evaluate $s(t)$ we consider its time-averaged value over a measurement interval T,

$$\langle s(t)\rangle_T \equiv \frac{1}{T}\int_t^{t+T} s(t')\, \mathrm{d}t'. \tag{3.9}$$

This gives

$$\langle s(t)\rangle_T = \frac{x(t + T) - x(t)}{T} = \frac{\varepsilon^{-1/3}a_p(t)^{2/3}}{T}(1 - [v_R(t; T)]^{2/9}), \tag{3.10}$$

where (3.3) defines the volume ratio $v_R(t; T)$. Furthermore, we perform an ensemble average to get $\mathbb{E}\{\langle s(t)\rangle_T\}$, the expected time-averaged speed for an ensemble of

(independent) Lagrangian air particles. Noting that $\langle s(t)\rangle_T = 0$ if no fragmentation occurs over the interval T,

$$\mathbb{E}\{\langle s(t)\rangle_T\} = \frac{p_{\text{frag}}(a_p(t);T)}{\varepsilon^{1/3}a_p(t)^{-2/3}T}(1-\mathbb{E}\{[v_R(t;T)]^{2/9} \mid \text{frag}\}). \tag{3.11}$$

The no-hysteresis assumption, along with (2.4), gives

$$\mathbb{E}\{\langle s(t)\rangle_T\} = C_\Omega(We)\frac{1-\exp[-\Omega(a_p(t))T]}{\Omega(a_p(t))T}(1-\mathbb{E}\{[v_R(t;T)]^{2/9} \mid \text{frag}\}). \tag{3.12}$$

Recalling that, by assumption, these statistics are scale invariant, we introduce T^* and apply (3.6) to obtain

$$\mathbb{E}\{\langle s(t)\rangle_{T^*}\} = C_{\Omega,\infty}\frac{1-\exp[-C_{\Omega,\infty}T^*]}{C_{\Omega,\infty}T^*}\left[1-\bar{m}(T^*)\int_0^1 v^{*11/9}f_V^*(v^*;T^*)\,\mathrm{d}v^*\right]. \tag{3.13}$$

The limit $T^* \to 0$ gives the expected instantaneous speed,

$$\bar{s} \equiv \lim_{T^*\to 0}\mathbb{E}\{\langle s(t)\rangle_{T^*}\} = C_{\Omega,\infty}\left[1-\bar{m}\int_0^1 v^{*11/9}f_V^*(v^*)\,\mathrm{d}v^*\right], \tag{3.14}$$

where $\bar{m}$ and $f_V^*(v^*)$ describe the fragmentation statistics for $T^* \to 0$ and are equivalent to those in (2.1).

Hereafter, we refer to $\bar{s}$ as the volume-propagation speed of a fragmentation cascade. Although the size locations of individual Lagrangian air particles in the cascade follow step functions, by commuting time averaging and ensemble averaging, we are able to obtain an average instantaneous speed for particles in the cascade. This speed $\bar{s}$ can be related to fragmentation statistics measured over finite intervals T (3.13), or the instantaneous statistics used by PBE (3.14). The relationship between the two is explored in § 3.4. In § 3.3 we use $\bar{s}$ to provide τ_c.

3.3. *Describing convergence time, τ_c*

As intended, our choice of the definition of location within the cascade, $x(t)$, makes $\bar{s}$ constant for $a_p(t) > a_H$. This constant speed means that, despite $x(t)$ being a step function, after a sufficient number of steps, we can treat fragmentation as a continuous process and apply the approximation $x(t) \approx t\bar{s}$ with reasonable (statistical) accuracy. Thus, we can approximate τ_c as the distance in x between a_{max} and a_H divided by this speed,

$$\tau_c = \frac{\left(\varepsilon^{-1/3}{a_{max}}^{2/3}\right) - \left(\varepsilon^{-1/3}{a_H}^{2/3}\right)}{\bar{s}}. \tag{3.15}$$

Non-dimensionalising $\tau_c^* = \tau_c\,\varepsilon^{1/3}{a_{max}}^{-2/3}$ and defining We_{max} to be the We associated with a_{max},

$$\tau_c^* = C_\tau[1-(We_{max}/We_H)^{-2/5}]; \quad C_\tau \equiv 1/\bar{s}. \tag{3.16a,b}$$

Despite the approximation used to derive (3.15) from $\bar{s}$ in (3.14), (3.16) is expected to be valid for $We^* = We_{max}/We_H$ not small (where multiple fragmentation events are generally necessary to reach a_H). This is confirmed by Monte Carlo simulations of prescribed fragmentation statistics (figure 2).

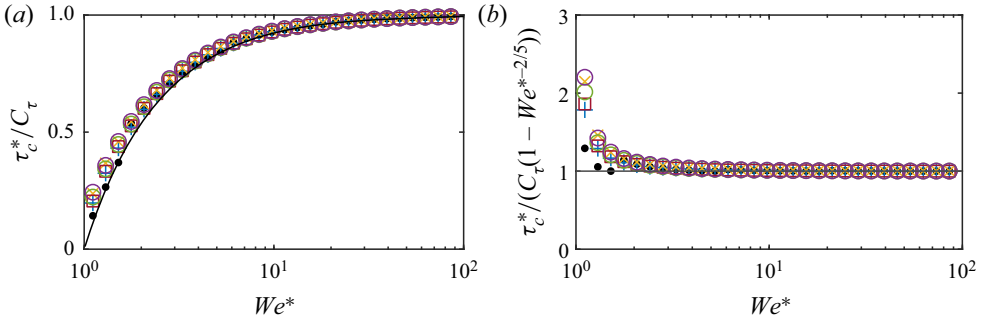

Figure 2. The effect of We^* on τ_c^* as modelled by (3.16) (solid line) compared with Monte Carlo simulations of daughter distributions: •, A; +, blue, B; ×, yellow, C; □, red, D; ○, green, E; ○, violet, F (see table 1), where (3.1) is used to model the Hinze scale. The 95 % confidence interval on all τ_c^* is $< 1\,\%$.

For $We \sim \infty$ we recover the same $\tau_c \propto \varepsilon^{-1/3} {a_{max}}^{2/3}$ scaling as previous work which assumes identical fragmentation (Deike *et al.* 2016). This scaling of τ_c is like τ_ℓ, demonstrating that the fragmentation rate is a dominant factor in determining τ_c. Our propagation speed-based analysis provides the scaling constant C_τ which quantifies the contribution of fragmentation rate, as well as fragmentation statistics $\bar{m}$ and $f_V^*(v^*)$. For large-but-finite *We*, (3.16) captures the effect of the *We*-driven separation between a_{max} and a_H on the value of τ_c; however, we note that the scaling or τ_c with *We* will be more complex for small *We* ($We \sim We_H$) as we have not incorporated the effect of finite-*We* on fragmentation rate, such as modelled by (2.5), into our propagation speed-based analysis. In § 4.5, DNS shows for what sufficiently large *We* this effect is negligible.

Although primarily driven by fragmentation rate, τ_c is also related to the fragmentation statistics $\bar{m}$ and $f_V^*(v^*)$ (Qi *et al.* 2020), which is now quantified by the scaling constant C_τ. To describe these relationships, we follow Gaylo *et al.* (2021) and isolate the effect of f_V^* from $\bar{m}$ through a daughter-distribution constant C_f, defined as the ratio between C_τ and a C_τ found using the same $\bar{m}$ but identical fragmentation, $f_V^*(v^*) = \delta(v^* - 1/\bar{m})$, where δ is the Dirac delta function. This gives

$$C_\tau = \frac{C_f / C_{\Omega,\infty}}{1 - \bar{m}^{-2/9}}; \quad C_f = \frac{1 - \bar{m}^{-2/9}}{1 - \bar{m} \int_0^1 {v^*}^{11/9} f_V^*(v^*)\,\mathrm{d}v^*}. \tag{3.17a,b}$$

In table 1 we compare this C_f for general fragmentation cascades to the similar constant (hereafter denoted as $C_f{}^\star$) derived by Gaylo *et al.* (2021) for the special case of power-law entrainment. The values are nearly equivalent, and, noting that $(9/2)(\ln \bar{m})^{-1} \approx (1 - \bar{m}^{-2/9})^{-1}$, (3.17) predicts similar τ_c as Gaylo *et al.* (2021) for their special case.

3.4. *Measurement-interval independence of volume-propagation speed*

A consequence of $\bar{s}$ being constant for $a_p(t) > a_H$ is that the time-averaged value and the instantaneous speed are equal, $\mathbb{E}\{\langle s(t)\rangle_T\} = \bar{s}$, so long as $a_p(t+T) > a_H$. Thus, to obtain $\bar{s}$ we must choose a T such that $\Pr\{a(t+T) > a_H\} \approx 1$. For measurements of an initial parent-bubble radius $a = a_p(t)$, we define an upper bound T_U as the interval we expect $a_p(t+T_U) \sim a_H$ and require $T \ll T_U$. Through the same arguments used to derive τ_c, this upper bound is

$$T \ll \varepsilon^{-1/3} a^{2/3} C_\tau [1 - (We/We_H)^{-2/5}], \tag{3.18}$$

or simply $T \ll \tau_c$ for $a = a_{max}$. From Monte Carlo simulations of prescribed fragmentation statistics measuring initial bubbles $a = a_{max}$, figure 3 confirms that $\mathbb{E}\{\langle s\rangle_T\}$

Label	Daughter distribution	m	$f_V^*(v^*)$	C_f	$C_f^\star$
A	Valentas, Bilous & Amundson (1966)	2	$\delta(v^* - 1/2)$	1	1
B	Martínez-Bazán, Montañés & Lasheras (1999*b*)	2	$(v^*)^{2/9}(1 - v^*)^{2/9}$	1.348	1.314
C	Tsouris & Tavlarides (1994)	2	$2^{1/3} - (v^*)^{2/3} - (1 - v^*)^{2/3}$	2.432	2.255
D	Martínez-Bazán *et al.* (2010)	2	$(v^*)^{-4/9}(1 - v^*)^{-4/9}$	1.782	1.712
E	Diemer & Olson (2002)	3	$(v^*)^{1/4}(1 - v^*)^{3/2}$	1.269	1.253
F	Diemer & Olson (2002)	4	$(v^*)^{1/2}(1 - v^*)^{7/2}$	1.190	1.185

Table 1. Daughter distributions used in Monte Carlo simulations and corresponding daughter-distribution constants C_f defined by (3.17) versus $C_f^\star$ defined by Gaylo *et al.* (2021, (4.3)). Note, a constant to ensure $\int f_V^*(v^*)\,\mathrm{d}v^* = 1$ is omitted for brevity.

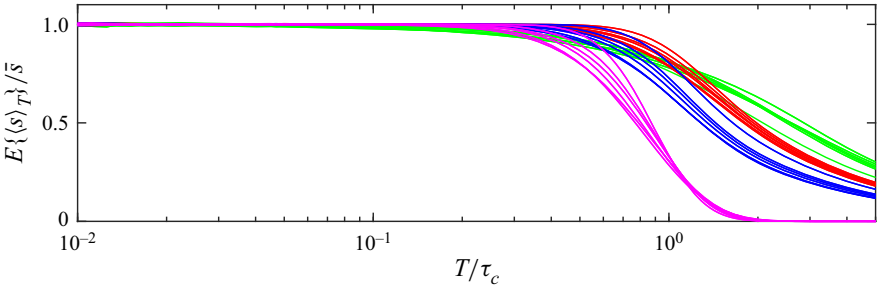

Figure 3. Measurements of $\mathbb{E}\{\langle s\rangle_T\}$ from Monte Carlo simulations of daughter distributions A–F (see table 1) at a range of T/τ_c, normalised by $\bar{s}$ calculated using (3.14). Colours based on *We**: green, 2; red, 50; blue, 100; magenta, 200, where (3.1) is used to model the Hinze scale. The 95 % confidence interval on $\mathbb{E}\{\langle s\rangle_T\}$ for $T/\tau_c < 1$ is < 3 %.

gives an exact, T-independent measurement of $\bar{s}$ for $T \ll \tau_c$. T_U provides an upper bound on T for experiments or simulations, although we point out that it is an *a posteriori* measure because C_τ is derived from $\bar{s}$.

Finally, T-independence means $\mathrm{d}\mathbb{E}\{\langle s(t)\rangle_T\}/\mathrm{d}T = 0$. As can been seen by taking the derivative of (3.13) with T^*, this bounds how scale-invariant fragmentation statistics $\bar{m}(T^*)$ and $f_V^*(v^*; T^*)$ can depend on T^* and provides insight into the relationship between $\bar{m}(T^*)$ and $f_V^*(v^*; T^*)$ measured at large T^* versus the theoretical $T^* \to 0$ limiting case used in PBE. This is useful because a finite relaxation time τ_r implies a lower bound ($T > \tau_r$) for measuring fragmentation statistics that are compatible with the PBE no-hysteresis assumption.

4. Quantification of fundamental time scales using DNS

We perform DNS of populations of bubbles fragmenting in HIT to measure the relaxation time τ_r and bubble lifetime τ_ℓ, validate the T-independence of measurements of $\bar{s}$, and provide a value of C_τ along with the minimum *We* above which this value is valid. A summary of the DNS performed is provided in table 2.

4.1. *Methodology*

For DNS, we solve the three-dimensional, incompressible, immiscible, two-phase, Navier–Stokes equations using a second-order finite-volume scheme on a uniform

We_T	We	Δ/η	We_Δ	Δ/a_H	N_{sims}	N_{frag}	C_Ω	C_τ
400	101–142	1.1	0.66	0.71	7	213	1.64 ± 0.42	8.9 ± 1.9
200	50 – 71	2.2	0.66	0.93	7	106	0.60 ± 0.13	16.1 ± 2.9
		1.5	0.44	0.62	7	189	1.21 ± 0.34	10.2 ± 2.5
		1.1	0.33	0.47	7	208	1.64 ± 0.44	9.8 ± 2.8
		0.7	0.22	0.31	5	187	1.77 ± 0.26	10.3 ± 2.1
100	25–36	1.1	0.16	0.31	7	218	1.50 ± 0.27	10.0 ± 2.3
50	13–18	1.1	0.08	0.20	7	174	0.93 ± 0.13	15.2 ± 2.9
25	6.3–8.9	1.1	0.04	0.13	7	113	0.44 ± 0.12	27.1 ± 5.5

Table 2. Summary of HIT simulations performed and values measured using $T/t_\ell = 0.4$, including 95 % confidence interval. Here N_{sims} is the number of simulations (each with different initial bubble populations) and N_{frag} is the total number of fragmentation events. Here a_H is calculated using $We_H \approx 7$ from § 4.4.

Cartesian grid. Phases are captured by the conservative volume-of-fluid method (Weymouth & Yue 2010), and surface tension is calculated using a height-function-based continuous-surface-force method (Popinet 2009). More detail on the DNS solver is provided by Campbell (2014) and Yu *et al.* (2019). During the simulation, normals-based informed component labelling (Hendrickson, Weymouth & Yue 2020) identifies bubbles, the air volumes of which are then tracked using Eulerian label advection (ELA) (Gaylo *et al.* 2022).

To develop the initial turbulent velocity field for the simulation, we use a linear forcing method (Lundgren 2003; Rosales & Meneveau 2005) on a triply periodic cubic domain, length $L = 5.28$, to develop single-phase HIT with a (non-dimensionalised) characteristic turbulent dissipation rate $\varepsilon = 1$, velocity fluctuation $u_{rms} = 1$ and Reynolds number $Re_T = u_{rms}^4/\varepsilon\nu_w = 200$. Using the single-phase HIT as the initial velocity field, we perform simulations with an ensemble of different initial air–water bubble populations (density ratio $\rho_w/\rho_a = 1000$, viscosity ratio $\mu_w/\mu_a = 100$, void fraction 1 %) at a range of turbulent Weber numbers, $We_T = \rho_w u_{rms}^5/\varepsilon\sigma$. Although the abrupt introduction of bubbles to single-phase HIT is non-physical, numerical simulations rapidly adjust (Yu *et al.* 2019; Rivière *et al.* 2021). Populations are created by randomly distributing (without overlap) spherical bubbles with radii between $3L/256$ and $15L/256$ following $N(a) \propto a^{-10/3}$. By repeating the random generation and distribution of bubble populations in the initial HIT velocity field, unique but statistically similar initial bubble populations are generated to provide statistical variation between our ensemble simulations.

During the evolution, linear forcing is applied to regions of water to maintain $\varepsilon \approx 1$ (Rivière *et al.* 2021). Figure 4 shows the evolution of a sample simulation and figure 5 shows the evolution of the ensemble bubble-size distribution both for $We_T = 100$. We note that, with our focus on bubbles $a > a_H$, the transition to a distinct a power-law regime for $N(a < a_H)$ is not captured (Deane & Stokes 2002). Over a measurement interval t^n to $t^{n+1} = t^n + T$, ELA provides the unique, volume-conservative volume-tracking matrix, where each element a_{ij} describes the volume that moved from a parent bubble j that is identified at t^n to a bubble i identified at t^{n+1} (Gaylo *et al.* 2022). From volume-tracking matrices, fragmentation statistics $\mathbb{E}\{\langle s\rangle_T\}$ and $p_{\text{frag}}(a;T)$ can easily be computed. We study fragmentation statistics for parent bubbles of radii $a_0 < a < 1.2a_0$, where $a_0 = 7L/256$ provides a balance between the number of observed fragmentation events per

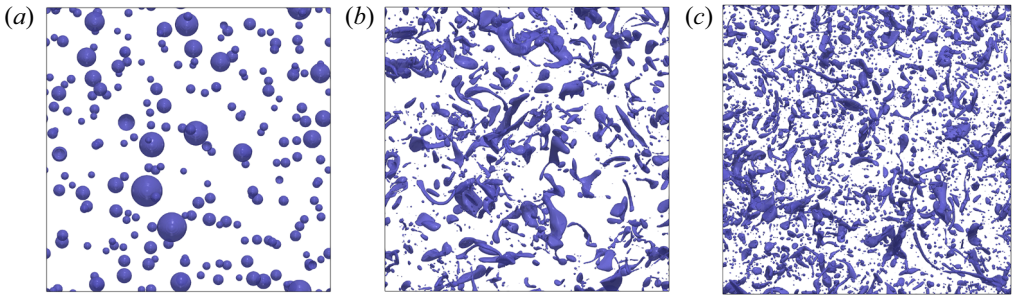

Figure 4. Volume-of-fluid $f = 0.5$ isosurface for one of the $We_T = 100$ simulations at (*a*) $t/t_\ell = 0$; (*b*) $t/t_\ell = 1$; (*c*) $t/t_\ell = 3$.

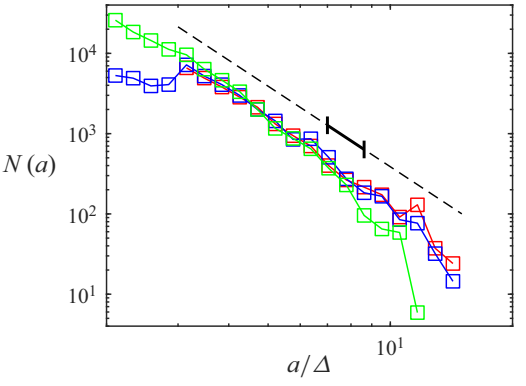

Figure 5. Average bubble-size distribution $N(a)$ for $We_T = 100$ simulations at times: red, $t/t_\ell = 0$; blue, $t/t_\ell = 1$; green, $t/t_\ell = 3$. Here $N(a) \propto a^{-10/3}$ is provided for reference over the range of initialised spherical bubbles (dashed line) and the range of measured parent bubbles, $a_0 < a < 1.2a_0$ (solid line).

simulation and resolution of the daughter bubbles. While this simulation is inherently transient, figure 5 illustrates that for this range of bubbles a quasisteady period exists. By initialising the bubbles to follow an equilibrium fragmentation cascade $N(a) \propto a^{-10/3}$ (Garrett *et al.* 2000), the fragmentation of bubbles $a > a_0$ maintains the population of bubbles $a \sim a_0$ for $t/t_\ell < 3$, where $t_\ell = (0.42)^{-1}\varepsilon^{-1/3}{a_0}^{2/3}$ is an *a priori* estimate of τ_ℓ (Martínez-Bazán *et al.* 1999*a*). To exclude the fragmentation of the initial set of spherical bubbles (see figure 4), we study fragmentation over $1 < t/t_\ell$. Thus, by measuring fragmentation statistics over $1 < t/t_\ell < 3$, we measure a quasisteady population of parent bubbles that are realistically formed by a fragmentation cascade.

4.2. *Grid independence*

The choice of cell size, Δ, is driven by resolving the relevant scales of turbulence and surface tension. For turbulence, we compare the grid with the Kolmogorov microscale, $\eta \sim \varepsilon^{-1/4}{\nu_w}^{3/4}$, where $\Delta/\eta \lesssim 1$ ensures turbulence is resolved. For surface tension, we consider the cell Weber number $We_\Delta = \rho_w u_{rms}^2 \Delta/4\pi\sigma$, which estimates the ratio between the grid and the minimum characteristic radius of curvature of an interface deformed by inertial turbulence. Here $We_\Delta < 1$ ensures surface tension forces are resolved by the grid (Popinet 2018). We also consider Δ/a_H, comparing the grid to the Hinze scale: with

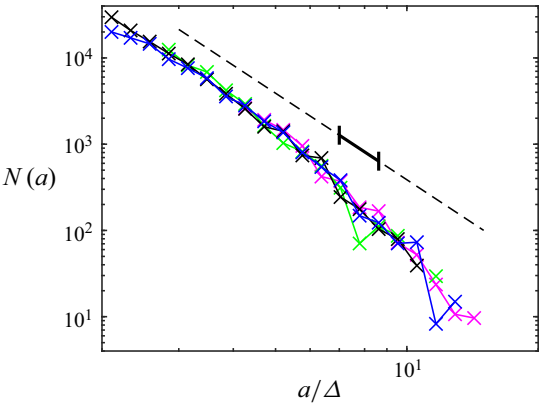

Figure 6. Average bubble-size distribution $N(a > 2\Delta)$ for $We_T = 200$ at time $t/t_\ell = 3$ from simulations with grids: magenta, $L/\Delta = 128$; green, $L/\Delta = 192$; black, $L/\Delta = 256$; blue, $L/\Delta = 384$. Horizontal axis is normalised by $\Delta = L/256$ and $N(a) \propto a^{-10/3}$ is provided for reference over the range of initialised spherical bubbles (dashed line) and the range of measured parent bubbles, $a_0 < a < 1.2a_0$ (solid line).

ε and u_{rms} fixed ${We_\Delta}^{3/5} \propto \Delta/a_H$. Based on these metrics we find $L/\Delta = 256$ resolves turbulence and surface tension for our entire range of We_T (see table 2).

With no clear lower limit to the ratio between the daughter-bubble and parent-bubble volume (v^*), grid resolution limitations require us to filter out daughter bubbles of radius $a < 2\Delta$. Figure 6 shows that the bubble-size distribution of filtered bubbles, $N(a > 2\Delta)$, is grid-independent. For $L/\Delta = 256$ and parent bubbles $a_0 = 7L/256$, $a < 2\Delta$ corresponds to $v^* < 0.02$. While this filter prevents us from measuring the full range of possible daughter bubbles, especially sub-Hinze daughters, we expect this to have little effect on the statistics of interest for two reasons. First, sub-Hinze bubble production by fragmentation happens concurrently with the production of large daughter bubbles (Rivière *et al.* 2022), so excluding small daughters should not affect the measured rate of fragmentation used to obtain τ_r and τ_ℓ. Second, for τ_c, the integral of the daughter-size distribution in (3.17) weights local daughter production ($v^* \sim 1/\bar{m}$) over non-local daughter production ($v^* \ll 1$), making the contribution of the excluded small daughters small. This is related conceptually to locality, which suggests $v^* \ll 1$ can be neglected when modelling the cascade (Chan *et al.* 2021*b*,*c*).

To confirm that we resolve turbulence and surface tension, that the filter has a negligible effect, and (more broadly) that the statistics we measure are independent of the grid, we perform a convergence study for $We_T = 200$ using three additional grids, $L/\Delta = 128$, 192 and 384. The results of this convergence study (see figure 7) show that our measurements of fragmentation statistics $\mathbb{E}\{\langle s \rangle_T\}$ and $p_{\text{frag}}(a; T)$ (from which the time scales will be calculated) are grid independent for $L/\Delta \geq 256$.

4.3. *Estimating relaxation time, τ_r*

For each simulation, we use six instances of ELA with different measurement intervals T. Using (2.4) and (2.7), we calculate $C_\Omega(We; T)$ from each $p_{frag}(a; T)$. Figure 8(*a*) shows how T affects the measured value of C_Ω, where we use $T/t_\ell = 0.4$ as a reference value for each We. If the no-hysteresis assumption were valid for all T, C_Ω would be a constant for each We. Figure 8(*a*), however, shows a strong dependence on small T. We observe that this dependence is approximately exponential, which provides an empirical definition of

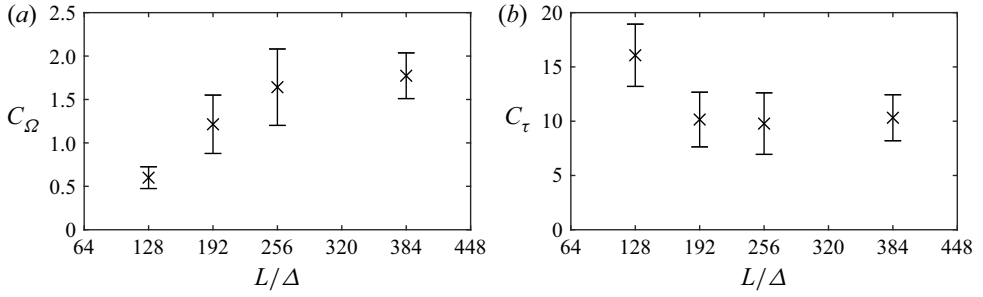

Figure 7. Grid-convergence study for (*a*) fragmentation rate constant C_Ω and (*b*) convergence constant C_τ based on simulations of $We_T = 200$ (parent bubbles $We = 50$–71) with different grids, measured using $T/t_\ell = 0.4$. Error bars indicate 95 % confidence interval.

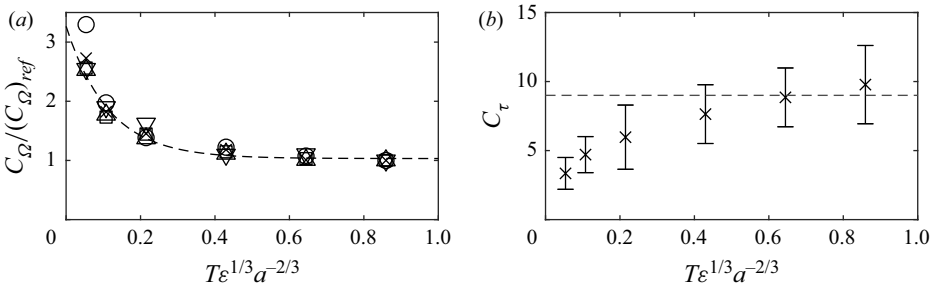

Figure 8. Measured (*a*) fragmentation-rate constant C_Ω normalised by $(C_\Omega)_{ref}$, the value measured using $T/t_\ell = 0.4$ and (*b*) the convergence constant C_τ for *We* of (○) 101–142; (×) 50–71; (□) 25–36; (△) 13–18; (▽) 6.3–8.9. In (*a*), variance-weighted least-squares fit of all data to (4.1) (dashed line) gives $C_r = 0.11$ and $A = 2.2$ ($R^2 = 0.954$). In (*b*), error bars indicate 95 % confidence interval and the estimated large-*We* value of $C_\tau = 9$ (dashed line) is included for reference.

the relaxation time τ_r as well as the hysteresis strength A:

$$C_\Omega(We; T)/C_\Omega(We; T \sim \infty) = 1 + A\exp[-T/\tau_r]. \tag{4.1}$$

We observe that τ_r scales like τ_ℓ rather than, say, bubble natural period, $We^{-1/2}\varepsilon^{-1/3}a^{2/3}$. Thus, we define the scaling constant C_r and write $\tau_r = C_r\varepsilon^{-1/3}a^{2/3}$. This scaling suggests that, for $We > We_H$, the physical mechanisms for the decay of hysteresis are not related to surface tension. Future, more detailed, studies of the dynamics of individual bubbles are necessary to understand hysteresis and identify the mechanisms for its decay. For our statistical study, our concern is to determine when hysteresis can be neglected. Least-squares regression of the combined data for all *We* gives $C_r \approx 0.11$. Hereafter, we measure all results with $T/t_\ell = 0.4$ (corresponding to $T/\tau_r \approx 8$), which guarantees that effect of hysteresis on our estimation of τ_ℓ and τ_c is negligible.

4.4. *Estimating bubble lifetime, τ_ℓ*

We now seek the expected bubble lifetime, τ_ℓ. Figure 9(*a*) shows our measurements of $C_\Omega(We)$ and their fit to (2.5). We find the Hinze-scale $We_H = 6.9$, similar to $We_H = 4.7$ measured by Martínez-Bazán *et al.* (1999*a*) and $We_H = 2.7$–7.8 by Risso & Fabre (1998). However, we obtain $C_{\Omega,\infty} = 1.4$, greater than $C_{\Omega,\infty} = 0.42$ measured by Martínez-Bazán *et al.* (1999*a*) and $C_{\Omega,\infty} = 0.95$ from HIT simulations by Rivière

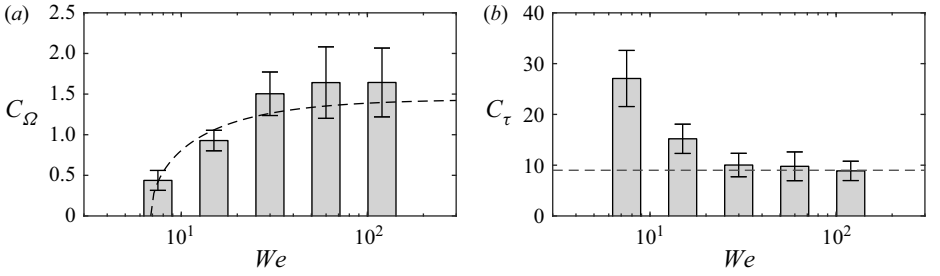

Figure 9. (*a*) Fragmentation rate constant C_Ω and (*b*) convergence constant C_τ as functions of *We*, measured using $T/t_\ell = 0.4$. Error bars indicate 95 % confidence interval. In (*a*), variance-weighted least-squares fit to (2.5) (dashed line) gives $We_H = 6.9$ and $C_{\Omega,\infty} = 1.4$ ($R^2 = 0.890$). In (*b*), the estimated large-*We* value of $C_\tau = 9$ (dashed line) is included for reference.

et al. (2021). An important distinction between our fragmentation rate measurements and previous experimental and numerical measurements is that we measure bubbles that have been formed as the daughters of previous fragmentation, so the bubbles are already distorted by fragmentation. The effect of this distinction can be demonstrated by measuring the fragmentation statistics over an earlier time in our simulation, $0 < t/t_\ell < 1$, when (as opposed to the later time $1 < t/t_\ell < 3$) many parent bubbles which started spherical have not yet fragmented. When we measure this earlier time range (denoted by $(\cdot)_{t<t_\ell}$), we obtain a similar $(We_H)_{t<t_\ell} = 7.0$ but an appreciably smaller $(C_{\Omega,\infty})_{t<t_\ell} = 0.88$ ($R^2 = 0.974$). As our interest is bubbles within fragmentation cascades, our value of $C_{\Omega,\infty} \approx 1.4$ is more relevant for bubbles formed by fragmentation. Note that $1/C_{\Omega,\infty}$ is an order of magnitude larger than C_r (i.e. $\tau_\ell \gg \tau_r$), which confirms that the PBE no-hysteresis assumption is reasonable when modelling fragmentation cascades.

4.5. *Estimating convergence time, τ_c*

We now seek the convergence time, τ_c. As shown in § 3, the time-averaged speed $\mathbb{E}\{\langle s\rangle_T\}$, available from ELA, gives a T-independent measurement of C_τ so long as (3.18) is satisfied. Figure 9(*b*) shows the value of C_τ we obtain over a range of *We*. We find that the model developed in § 3, which as a result of large-*We* assumptions predicts a constant C_τ, is accurate for $We \gg We_H$, or more specifically $We > 30$, where we measure $C_\tau \approx 9$. To validate that our measurement is T-independent, we also measure C_τ using a range of T for $We = 50$–71 (figure 8*b*). As expected, for $T \lesssim \tau_r$ we see a dependence on T due to hysteresis, but for $T \gg \tau_r$ C_τ is independent of T. Using $C_\tau = 9$, (3.18) gives $T/T_U < 0.2$ for $We > 30$, so we do not expect any effect of the Hinze scale driven upper bound on T-independence described in § 3.4.

5. Discussion

We now examine how the relaxation time τ_r, bubble lifetime τ_ℓ and convergence time τ_c inform the study of fragmentation. For τ_r, our results suggest that the physical mechanism for the decay of hysteresis with bubble age is independent of surface tension for $We > We_H$ and that τ_r scales like τ_ℓ. The respective scaling constants we estimate from DNS of HIT differ by an order of magnitude ($C_r \ll 1/C_{\Omega,\infty}$), suggesting that $\tau_r \ll \tau_\ell$ is always true for $We > We_H$. Although the physical mechanism for the decay of hysteresis is unclear, this shows that hysteresis can be assumed negligible when modelling fragmentation, validating an essential assumption of PBE. More practically, knowledge of τ_r also informs the choice

of measurement interval in experiments and simulations. Here $T \gg \tau_r$ makes the effect of hysteresis on measurements negligible, ensuring that the measured fragmentation statistics are compatible with PBE.

The insight that the convergence time τ_c provides into the evolution of the bubble-size distribution in fragmentation-dominated bubbly flows has been discussed by Qi *et al.* (2020) and Deike *et al.* (2016), and we have now quantified τ_c directly. For large *We* where the effect of surface tension on fragmentation rates is negligible, we find

$$\tau_c = C_\tau \varepsilon^{-1/3} {a_{max}}^{2/3} [1 - (We_{max}/We_H)^{-2/5}], \tag{5.1}$$

where We_{max} is the Weber number of the largest bubble in the cascade (radius a_{max}) and we estimate $C_\tau \approx 9$ and $We_H \approx 6.9$ from DNS. In addition, as we can now express τ_c in terms of realistic fragmentation statistics for $We > 30$, τ_c also informs large-*We* fragmentation models. Inspired by (2.3), we rearrange (3.17) to provide a new bound on a moment of the daughter-size distribution f_V^*:

$$\bar{m} \int_0^1 {v^*}^{11/9} f_V^*(v^*)\, \mathrm{d}v^* = 1 - (C_\tau C_{\Omega,\infty})^{-1}, \tag{5.2}$$

where our estimations of $C_\tau \approx 9$ and $C_{\Omega,\infty} = 1.4$ from DNS give 0.92 for the right-hand side of (5.2). For a physical interpretation, (2.3) bounds the relationship between daughter-size distributions and $\bar{m}$ to guarantee volume conservation, while (for $We > 30$) (5.2) bounds the relationship to match the empirical value of τ_c.

Many existing fragmentation models assume binary breakup ($\bar{m} = 2$). To evaluate how well these meet (5.2), we focus on the proposed daughter-size distributions through C_f, which includes the integral in (5.2). With $\bar{m} = 2$, $C_\tau \approx 9$ and $C_{\Omega,\infty} = 1.4$, we obtain $C_f \approx 1.8$. Because C_f indicates how much longer τ_c is compared with the case of identical fragmentation, this shows that τ_c is 1.8 times longer for fragmentation in HIT than what would be predicted if one assumes identical binary-fragmentation. Comparing with more realistic binary daughter-distributions (B–D in table 1), we see good agreement with the distribution proposed by Martínez-Bazán *et al.* (2010). We also compare with the binary daughter-distribution model by Qi *et al.* (2020, eq. (7)), which uses an experimentally constrained fitting parameter $\omega = 0.3$ designed to tune the value of τ_c. For their daughter-distribution model, (3.17) gives $C_f = 1.741$, in good agreement with our value of $C_f \approx 1.8$. Although we assume $\bar{m} = 2$ here for illustration, this analysis is applicable to any $\bar{m}$. Rather than attempting to compare the details of disparate fragmentation models, relating τ_c to the fragmentation statistics specified by these models allows us to directly compare the physical predictions each model makes regarding the evolution of the bubble-size distribution through a simple scalar quantity.

6. Conclusion

For air–water bubbly flows under HIT at moderate to large Weber numbers, we describe three fundamental time scales characterising the statistics of the evolution of the bubble-size distribution by fragmentation and the resulting fragmentation cascade. The prevalence of the observation of a $-10/3$ power-law in bubble-size distributions in bubbly flow for moderate and large *We* demonstrates the importance of fragmentation cascades to the bubble-size distribution, and these time scales directly support statistical modelling of fragmentation. Although our focus here is on statistical descriptions of fragmentation, the results here also help inform mechanistic study of fragmentation.

One fundamental time scale is the relaxation time τ_r which characterises the time after fragmentation over which hysteresis cannot be neglected. From DNS measurements, we provide an empirical definition of τ_r based on when measured fragmentation rates become independent of the measurement interval T. We find that $\tau_r = C_r\varepsilon^{-1/3}a^{2/3}$, where $C_r \approx 0.11$ independent of moderate/large *We*. This *We*-independence suggests the physical mechanism causing τ_r at these *We* is unrelated to surface tension. Although understanding hysteresis and its decay is an area of future work, by providing τ_r we identify the time scales over which hysteresis can be neglected.

A second fundamental time scale is the expected lifetime τ_ℓ of a bubble from formation by fragmentation to further fragmentation. For $\tau_\ell \gg \tau_r$, $\tau_\ell = [C_\Omega(We)]^{-1}\varepsilon^{-1/3}a^{2/3}$ is the inverse of the fragmentation rate. Fitting our DNS results for bubbles within the fragmentation cascade to the square-root model of *We*-dependence by Martínez-Bazán *et al.* (1999*a*) (2.5), we find the Hinze-scale $We_H \approx 6.9$, in agreement with previous experiments, but measure a smaller τ_ℓ corresponding to a higher scaling constant (at large *We*) $C_{\Omega,\infty} \approx 1.4$ (compared with $C_{\Omega,\infty} \approx 0.42$ reported by Martínez-Bazán *et al.* (1999*a*)). We show that this higher value of $C_{\Omega,\infty}$ is related to formation of the bubbles by a fragmentation cascade. For modelling fragmentation cascades, this higher $C_{\Omega,\infty}$ is likely more relevant. In either case, we find $\tau_r \ll \tau_\ell$ for all *We*, validating the use of the no-hysteresis assumption in modelling fragmentation.

Finally, we consider the fundamental time scale $\tau_c = C_\tau[1 - (We_{max}/We_H)^{-2/5}]\varepsilon^{-1/3}a_{max}^{2/3}$, which measures the time for a Lagrangian air particle to go from the largest bubble to the Hinze scale. This also characterises the time for fragmentation cascades to reach equilibrium. For large *We*, we derive τ_c based on the (constant) expected speed $\bar{s}$ at which a Lagrangian air particle moves through the cascade. We show that, $C_\tau = 1/\bar{s}$ and can thus be measured independent of T. This result is valid for $\tau_r \ll T \ll \tau_c$, which provides a bound on the choice of T in experiments and simulations. The T-independence of C_τ is confirmed by DNS measurements, which give $C_\tau \approx 9$ for $We > 30$, which agrees well with the values obtained from the fragmentation model of Martínez-Bazán *et al.* (2010) and an experimentally constrained fragmentation model of Qi *et al.* (2020). The relationship between C_τ and fragmentation statistics in PBE provides new constraints on these statistics, at large *We*, limiting the possible forms of fragmentation models. Further, by quantifying C_τ, we obtain the convergence time of fragmentation cascades τ_c, beyond which a quasisteady model of fragmentation would be appropriate.

Funding. This work was funded by the US Office of Naval Research grant N00014-20-1-2059 under the guidance of Dr W.-M. Lin. The computational resources were funded through the Department of Defense High Performance Computing Modernization Program.

Declaration of interests. The authors report no conflict of interest.

Author ORCIDs.
Declan B. Gaylo https://orcid.org/0000-0001-6198-7003;
Kelli Hendrickson https://orcid.org/0000-0002-3596-6556;
Dick K.P. Yue https://orcid.org/0000-0003-1273-9964.

References

Campbell, B. 2014 A mechanistic investigation of nonlinear interfacial instabilities leading to slug formation in multiphase flows. PhD thesis, Massachusetts Institute of Technology, Cambridge, MA.

Castro, A.M. & Carrica, P.M. 2013 Bubble size distribution prediction for large-scale ship flows: model evaluation and numerical issues. *Intl J. Multiphase Flow* **57**, 131–150.

CHAN, W.H.R., DODD, M.S., JOHNSON, P.L. & MOIN, P. 2021*a* Identifying and tracking bubbles and drops in simulations: a toolbox for obtaining sizes, lineages, and breakup and coalescence statistics. *J. Comput. Phys.* **432**, 110156.

CHAN, W.H.R., JOHNSON, P.L. & MOIN, P. 2021*b* The turbulent bubble break-up cascade. Part 1. Theoretical developments. *J. Fluid Mech.* **912**, A42.

CHAN, W.H.R., JOHNSON, P.L., MOIN, P. & URZAY, J. 2021*c* The turbulent bubble break-up cascade. Part 2. Numerical simulations of breaking waves. *J. Fluid Mech.* **912**, A43.

DEANE, G.B. & STOKES, M.D. 2002 Scale dependence of bubble creation mechanisms in breaking waves. *Nature* **418**, 839–844.

DEIKE, L. 2022 Mass transfer at the ocean–atmosphere interface: the role of wave breaking, droplets, and bubbles. *Annu. Rev. Fluid Mech.* **54** (1), 191–224.

DEIKE, L., MELVILLE, W.K. & POPINET, S. 2016 Air entrainment and bubble statistics in breaking waves. *J. Fluid Mech.* **801**, 91–129.

DIEMER, R.B. & OLSON, J.H. 2002 A moment methodology for coagulation and breakage problems. Part 3. Generalized daughter distribution functions. *Chem. Engng Sci.* **57**, 4187–4198.

GARRETT, C., LI, M. & FARMER, D. 2000 The connection between bubble size spectra and energy dissipation rates in the upper ocean. *J. Phys. Oceanogr.* **30** (9), 2163–2171.

GAYLO, D.B., HENDRICKSON, K. & YUE, D.K.P. 2021 Effects of power-law entrainment on bubble fragmentation cascades. *J. Fluid Mech.* **917**, R1.

GAYLO, D.B., HENDRICKSON, K. & YUE, D.K.P. 2022 An Eulerian label advection method for conservative volume-based tracking of bubbles/droplets. *J. Comput. Phys.* **470**, 111560.

HENDRICKSON, K., WEYMOUTH, G.D. & YUE, D.K.P. 2020 Informed component label algorithm for robust identification of connected components with volume-of-fluid method. *Comput. Fluids* **197**, 104373.

HINZE, J.O. 1955 Fundamentals of the hydrodynamic mechanism of splitting in dispersion processes. *AIChE J.* **1**, 289–295.

LIAO, Y. & LUCAS, D. 2009 A literature review of theoretical models for drop and bubble breakup in turbulent dispersions. *Chem. Engng Sci.* **64**, 3389–3406.

LUNDGREN, T.S. 2003 Linearly forced isotropic turbulence. *Tech. Rep.* Center for Turbulence Research, Stanford University.

MARTÍNEZ-BAZÁN, C., MONTAÑÉS, J.L. & LASHERAS, J.C. 1999*a* On the breakup of an air bubble injected into a fully developed turbulent flow. Part 1. Breakup frequency. *J. Fluid Mech.* **401**, 157–182.

MARTÍNEZ-BAZÁN, C., MONTAÑÉS, J.L. & LASHERAS, J.C. 1999*b* On the breakup of an air bubble injected into a fully developed turbulent flow. Part 2. Size pdf of the resulting daughter bubbles. *J. Fluid Mech.* **401**, 183–207.

MARTÍNEZ-BAZÁN, C., RODRÍGUEZ-RODRÍGUEZ, J., DEANE, G.B., MONTAES, J.L. & LASHERAS, J.C. 2010 Considerations on bubble fragmentation models. *J. Fluid Mech.* **661**, 159–177.

POPINET, S. 2009 An accurate adaptive solver for surface-tension-driven interfacial flows. *J. Comput. Phys.* **228** (16), 5838–5866.

POPINET, S. 2018 Numerical models of surface tension. *Annu. Rev. Fluid Mech.* **50** (1), 49–75.

QI, Y., MOHAMMAD MASUK, A.U. & NI, R. 2020 Towards a model of bubble breakup in turbulence through experimental constraints. *Intl J. Multiphase Flow* **132**, 103397.

QI, Y., TAN, S., CORBITT, N., URBANIK, C., SALIBINDLA, A.K.R. & NI, R. 2022 Fragmentation in turbulence by small eddies. *Nat. Commun.* **13**, 469.

RISSO, F. & FABRE, J. 1998 Oscillations and breakup of a bubble immersed in a turbulent field. *J. Fluid Mech.* **372**, 323–355.

RIVIÈRE, A., MOSTERT, W., PERRARD, S. & DEIKE, L. 2021 Sub-Hinze scale bubble production in turbulent bubble break-up. *J. Fluid Mech.* **917**, A40.

RIVIÈRE, A., RUTH, D.J., MOSTERT, W., DEIKE, L. & PERRARD, S. 2022 Capillary driven fragmentation of large gas bubbles in turbulence. *Phys. Rev. Fluids* **7** (8), 083602.

ROSALES, C. & MENEVEAU, C. 2005 Linear forcing in numerical simulations of isotropic turbulence: physical space implementations and convergence properties. *Phys. Fluids* **17**, 095106.

SKARTLIEN, R., SOLLUM, E. & SCHUMANN, H. 2013 Droplet size distributions in turbulent emulsions: breakup criteria and surfactant effects from direct numerical simulations. *J. Chem. Phys.* **139**, 174901.

SOLSVIK, J., MAASS, S. & JAKOBSEN, H.A. 2016 Definition of the single drop breakup event. *Ind. Engng Chem. Res* **55**, 2872–2882.

SPORLEDER, F., BORKA, Z., SOLSVIK, J. & JAKOBSEN, H.A. 2012 On the population balance equation. *Rev. Chem. Engng* **28**, 149–169.

TSOURIS, C. & TAVLARIDES, L.L. 1994 Breakage and coalescence models for drops in turbulent dispersions. *AIChE J.* **40**, 395–406.

VALENTAS, K.J., BILOUS, O. & AMUNDSON, N.R. 1966 Analysis of breakage in dispersed phase systems. *Ind. Engng Chem. Fundam.* **5**, 271–279.

VEJRAŽKA, J., ZEDNÍKOVÁ, M. & STANOVSKÝ, P. 2018 Experiments on breakup of bubbles in a turbulent flow. *AIChE J.* **64**, 740–757.

WEYMOUTH, G.D. & YUE, D.K.P. 2010 Conservative volume-of-fluid method for free-surface simulations on Cartesian-grids. *J. Comput. Phys.* **229** (8), 2853–2865.

YU, X., HENDRICKSON, K., CAMPBELL, B.K. & YUE, D.K.P. 2019 Numerical investigation of shear-flow free-surface turbulence and air entrainment at large Froude and Weber numbers. *J. Fluid Mech.* **880**, 209–238.

YU, X., HENDRICKSON, K. & YUE, D.K.P. 2020 Scale separation and dependence of entrainment bubble-size distribution in free-surface turbulence. *J. Fluid Mech.* **885**, R2.